Downregulation of PIK3IP1/TrIP on T cells is controlled by TCR signal strength, PKC, and metalloprotease-mediated cleavage

Benjamin M. Murter[1,2], Sean C. Robinson[1], Hridesh Banerjee[1], Louis Lau[1,2], Uzodinma Uche[1], Andrea L. Szymczak-Workman[1], and Lawrence P. Kane[1]*

[1]Dept. of Immunology, University of Pittsburgh, Pittsburgh PA, USA

[2]Graduate Program in Microbiology and Immunology, University of Pittsburgh, Pittsburgh PA, USA

* To whom correspondence should be addressed: lkane@pitt.edu

Abstract

The protein known as PI3K-interacting protein (PIK3IP1), or transmembrane inhibitor of PI3K (TrIP), is highly expressed by T cells and can modulate PI3K activity in these cells. Several studies have also revealed that TrIP is rapidly downregulated following T cell activation. However, it is unclear as to how this downregulation is controlled. Using a novel monoclonal antibody that robustly stains cell-surface TrIP, we demonstrate that TrIP is lost from the surface of activated T cells in a manner dependent on the strength of signaling through the T cell receptor (TCR) and specific downstream signaling pathways. In addition, TrIP expression returns after 24 hours, suggesting that it may play a role in resetting TCR signaling at later time points. Finally, by expressing truncated forms of TrIP in cells, we identify the region in the extracellular stalk domain of TrIP that is targeted for proteolytic cleavage by metalloprotease ADAM17.

Keywords: T-cell, T-cell receptor (TCR), cell signaling, cellular immune response, phosphatidylinositide 3-kinase (PI 3-kinase), matrix metalloproteinase (MMP), ADAM, PIK3IP1, TrIP

Introduction

Signaling pathways controlled by phosphoinositide (PI) intermediates are ubiquitous regulators of cell growth, survival and transformation (1). Key signal transducers in this pathway include various phosphatidylinositol 3-kinases (PI3K), which catalyze phosphorylation of PI species at the 3' position of the inositol ring to produce PIP_3 and related species. The second messenger PIP_3 acts to recruit pleckstrin homology (PH) domain-containing proteins like Akt to the plasma membrane. In total, four different catalytic subunits ($\alpha, \beta, \gamma, \delta$) comprise the PI3K family, which pair with adaptor subunits that allosterically regulate PI3K activation (2–4). The major PI3K isoform linked to T cell activation is PI3Kδ. The PI3K signaling pathway is a significant mediator of activation, survival and differentiation signals downstream of the TCR and CD28, integrating antigen recognition and co-stimulatory signals, respectively (5–8). Additionally, IL-2 and IL-15 cytokine receptors also activate PI3Ks to modulate T cell survival and function (9). Counter-regulating these activating signals are several phosphatases, most notably the lipid-phosphatase and tumor suppressor PTEN, which regulate these signals and tune the T cell response (10). *In vivo*, dysregulation of PI3K signaling in T cells can lead to the development of hematological malignancy or immunodeficiency (11–13).

While it has long been known that PI3Ks are activated in response to TCR for antigen and co-stimulatory molecule (e.g. CD28) engagement, the precise role of this pathway in T cell responses has been more challenging to parse. Andreatti, et al. previously demonstrated that the PI3K signaling pathway plays a more nuanced role in T cell biology (14) when compared with the critical TCR-proximal kinases (Lck, Zap70) and adaptor proteins (LAT, SLP-76). Thus, a fuller understanding of the role of this pathway in T cell biology has required *in vivo* approaches, where more subtle mechanisms can be revealed through downstream effects on T cell differentiation.

We and others recently reported that T cell activation can be modulated by a novel negative regulator of PI3K that we have referred to as transmembrane inhibitor of PI3K (TrIP;

gene name *PIK3IP1*) (15–17). Unique among known negative regulators of PI3Ks, TrIP is a transmembrane protein that contains an SH2-homology domain toward its C-terminus similar to the inter-SH2 domain of p85α/β, which are critical upstream positive regulators of PI3K catalytic subunit (p110 family) activation. Although the precise molecular mechanism by which TrIP functions is not clear, evidence suggests that TrIP specifically interacts with p85 and is recruited to phospho-Tyr residues in proteins like CD28 and that interferes allosterically with the activation of p110 by p85. This interaction between TrIP and the p110/p85 heterodimer has been shown to negatively regulate the catalytic activity of PI3K and inhibit downstream signaling (18).

Although initial studies on TrIP shed light on its roles in T cell activation, they were somewhat limited by the lack of a suitable monoclonal antibody (mAb) that could assay cell-surface expression of TrIP. In this study, we detail the production and validation of such antibodies, focusing on the highest sensitivity mAb clone 18E10. We have used this antibody to characterize the levels of TrIP on various immune cell types, finding that neutrophils and $CD8^+$ T cells have particularly high expression. We confirm that endogenous cell-surface TrIP protein is lost upon TCR activation on $CD8^+$ T cells, discovering that this downregulation is related to strength of activating TCR signal. We also are the first to report that although highly expressed in naïve cells, TrIP expression on $CD8^+$ T cells does return at later time points following activation. Additionally, we have found that PKC activation downstream of TCR signaling is required to trigger the downregulation of TrIP surface expression. Furthermore, we have determined that matrix metalloproteases, specifically ADAM17, is responsible for the downregulation of endogenous TrIP protein from activated T cells. Finally, we have discovered that this downregulation is mediated by site-specific cleavage in the stalk domain. Taken together, these studies advance our knowledge of both how TrIP is regulated at the cellular level, and how this is tied to initiation of T cell activation. Finally, our identification of a non-cleavable form of TrIP should promote further understanding of the wider biological effects of this protein *in vivo*.

Results

Development of monoclonal antibodies to murine TrIP

The *in vivo* study of TrIP function has been hampered by the lack of suitable antibodies, especially against the extracellular domain of the protein. We therefore generated an Ig fusion protein by cloning the extracellular domain of TrIP into a vector encoding the Fc region from human IgG1 (TrIP-Ig; **Fig. 1A**). This construct was then used to produce recombinant TrIP-Ig by transfection into HEK293T cells. After confirming its integrity by SDS-PAGE (**Fig. 1B**), TrIP-Ig was used to immunize rats. Spleens of immunized rats were harvested and fused with myeloma cells to generate hybridomas. Supernatants from stable clones were then screened against TrIP-Ig and counter-screened against human IgG1. Supernatants from three sub-clones were then screened for the ability to recognize murine TrIP (mTrIP) by flow cytometry. Initially, HEK293T cells were transiently transfected with a Flag-tagged mTrIP (Flag-mTrIP) construct and labeled with supernatant from each anti-TrIP mAb clones. Following up with an anti-rat IgG secondary to label the clones with a fluorophore we show in **Figure 1C**, all three of these mAb's specifically bound to cells expressing Flag-mTrIP, showing double positive staining for flag as control. The degree of binding, however, varied by clone with 18E10 showing the most robust labeling of mTrIP based on co-labeling with an anti-Flag mAb (**Fig. 1C**). We also screened the anti-TrIP clones for cross-reactivity with human TrIP, as mouse and human TrIP are approximately 80% identical, and therefore could potentially cross-react (18). Although not seen with all three Ab's, we did find that the 18E10 clone displayed some cross-reactivity with human TrIP (**Fig. 1D**). We next determined which of the two major extracellular regions, the stalk domain or the kringle domain, the novel anti-TrIP mAb's were binding. To test this, we compared binding of the Ab's to full-length TrIP vs. a construct engineered to lack the kringle domain, but still bearing a N-terminal Flag tag on the stalk for detection. Despite robust Flag staining, binding of all the mAb's was lost in the absence of the kringle domain (mTrIP-ΔKringle) (**Fig. 1E**). These data demonstrate that we have

successfully generated several monoclonal anti-murine TrIP antibody clones, which bind via its kringle domain. Additionally, we found that that the most sensitive mAb (18E10) shows cross-reactivity with human-TrIP.

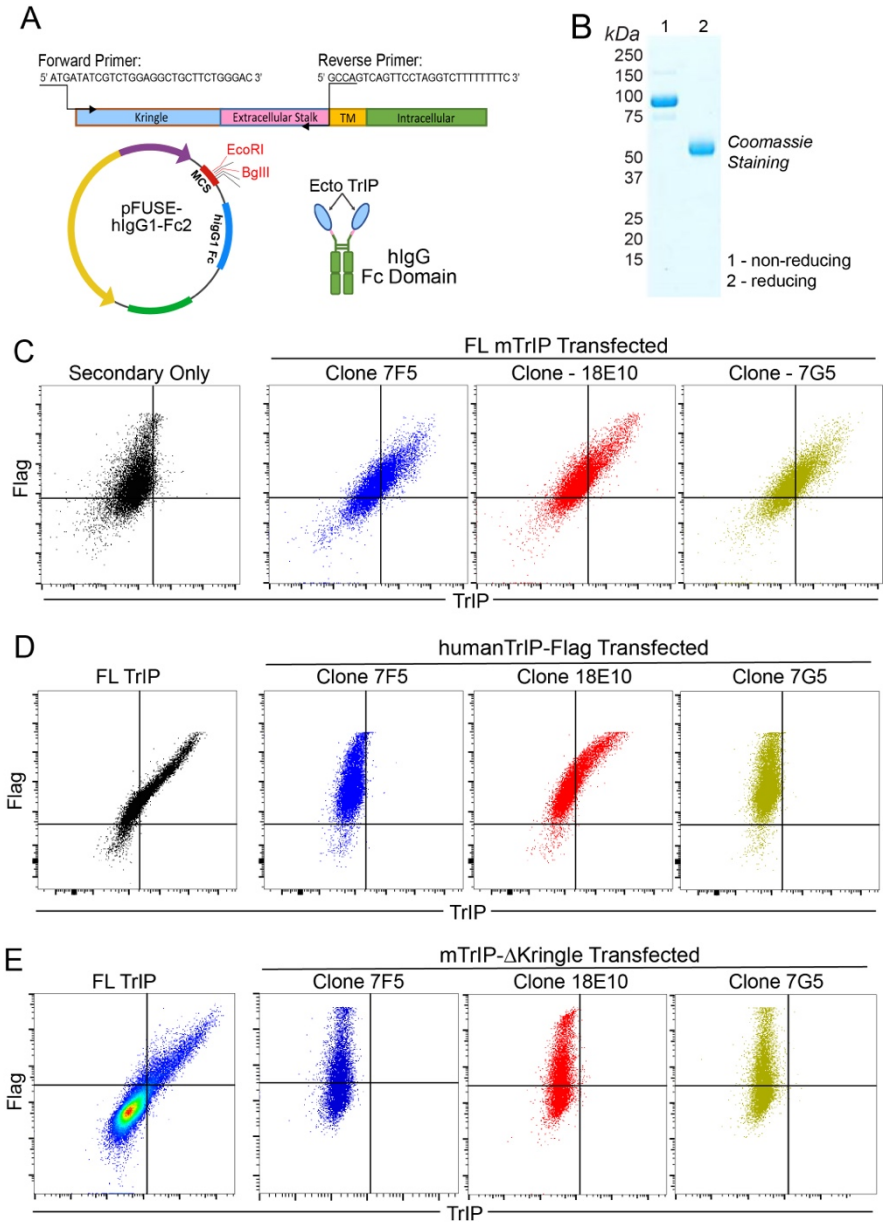

Figure 1. Development and validation of novel monoclonal antibodies to the ecto domain of TrIP. *A,* Cloning strategy and development of the ecto-TrIP Fc-fusion protein used for immunization and antibody development. *B,* SDS-PAGE of the ectoTrIP-Ig fusion protein under reducing and non-reducing conditions. *C,* Flow cytometry data showing the binding of each of 3 anti-TrIP monoclonal antibodies to a Flag-tagged WT murine TrIP construct expressed in HEK293T cells. *D,* Flow cytometry data showing staining of the 3 clones on HEK293T cells transfected with a plasmid encoding Flag-tagged human TrIP. *E,* Flow cytometry data showing the staining of each of the 3 anti-TrIP mAbs on HEK293T cells transfected with a Flag-tagged mTrIP construct lacking the extracellular kringle domain (ΔKringle).

Expression of TrIP on normal murine splenocytes

We next wanted to confirm that the newly generated anti-mTrIP mAb could recognize endogenous levels of protein. Thus, we directly conjugated anti-mTrIP mAb 18E10 to Alexa Fluor 647 for use in multi-color flow cytometry. Previous reports (17, 19, 20) and public data sets (21) show that TrIP expression is not restricted to just the T cell compartment. Therefore, we incorporated the 18E10 mAb in a large spectral flow cytometry panel for murine splenocytes to assess TrIP expression more broadly. Using the ExCYT software package (22), we performed high-dimensional clustering analysis (TSNE) of these data and were able to indentify a wide range of cell types (**Fig. 2A)**. Next, we overlayed the expression pattern of TrIP as a heatmap (**Fig. 2B**), which revealed expression across cell types, with especially robust expression on $CD8^+$ T cells ($CD3^+CD8^+$), whereas Treg ($CD3^+CD4^+Foxp3^+$) and conventional CD4 ($CD3^+CD4^+Foxp3^-$) had much lower expression in comparison (**Fig. 2C-D**). Of the major myeloid populations characterized, we did find moderate levels of TrIP expression on macrophages ($CD11b^+F4/80^+$) and the highest levels of TrIP expression were seen in the neutrophils ($CD11b^+Gr1^{Hi}$) (**Fig. 2C-D**). In parallel, we also labeled splenocytes from a CD8-specific TrIP knockout mouse (*TrIP*$^{fl/fl}$ x E8i^{Cre}), a mouse model previously generated in our lab, as a negative control (16). Thus, the 18E10 mAb robustly stained WT $CD8^+$ T cells from naïve C57BL/6 mice, but not those from CD8-specific TrIP KO mice (**Fig. 2E**) confirming the staining specificity and sensitivity to endogenous levels of the protein.

Previous work from our lab and others has suggested that TrIP expression is high on resting cells but is downregulated upon T cell activation (15–17). In support of these data, staining of endogenous TrIP revealed that over 90% of splenic $CD8^+$ T cells are $TrIP^+$ (**Fig. 2E, H**). Furthermore, subsetting these cells based on their activation status revealed that TrIP was indeed expressed at much lower levels on effector ($CD44^+$), vs. naïve/resting ($CD62L^+$) T cells (**Fig. 2F-G**). Our previous studies using cell line expression of epitope-tagged TrIP suggested that TrIP surface expression is lost upon activation (16), so we wanted to confirm that endogenous TrIP

protein behaves in a similar manner. To test this, we subjected WT P14 splenocytes to plate-bound anti-CD3/anti-CD28 stimulation, and followed the expression of TrIP with the 18E10-AF647 mAb out to 24 hours after stimulation. As shown in **Figure 2H-I**, TrIP surface expression was rapidly lost within the first two hours of stimulation and remained at very low levels for at least twelve hours. To date, it has been unclear when, or even if, TrIP expression re-occurs following T cell activation. As shown in **Figure 2H-I**, we found that CD8$^+$ T cells begin to re-express TrIP around 12-24 hours following activation.

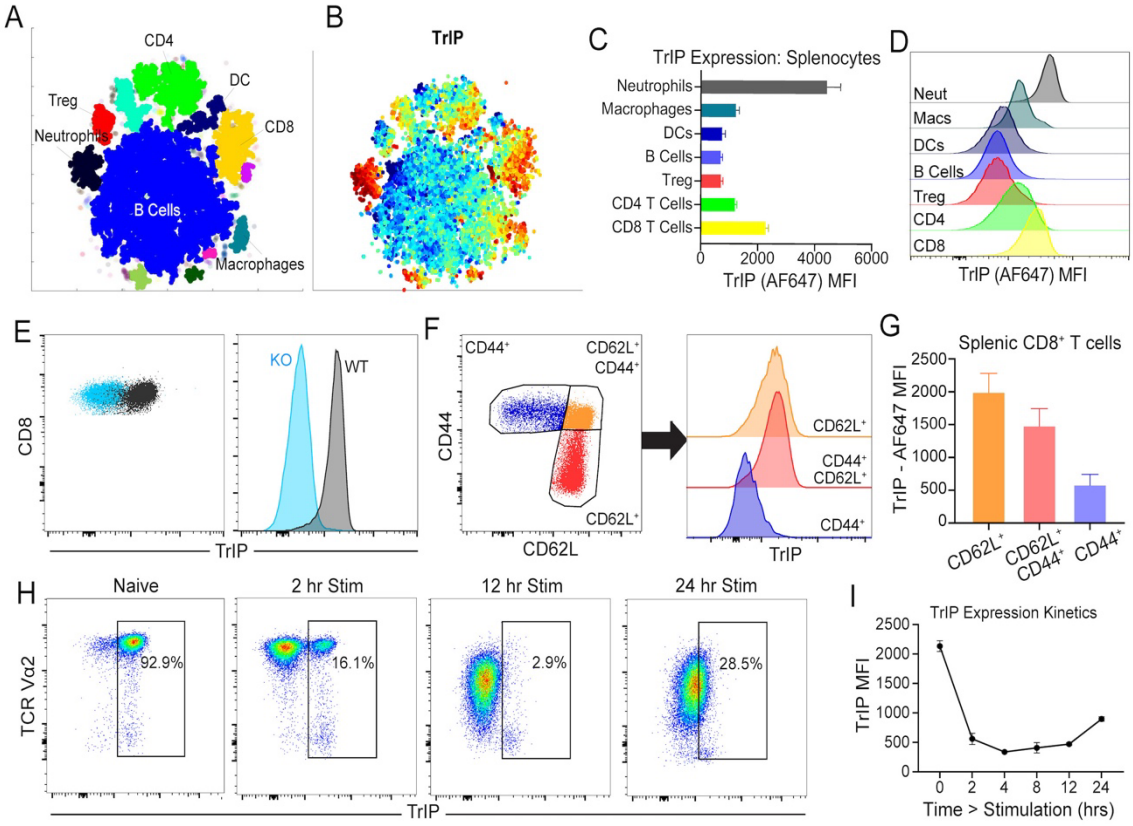

Figure 2. Characterization of TrIP expression on immune cells in naïve mice. *A*, ExCYT clustering analysis of flow cytometry data identifies major splenic populations including B cells (CD19$^+$), CD4 (CD3$^+$CD4$^+$FoxP3$^-$) and CD8 (CD3$^+$CD8$^+$) T cells, regulatory T cells (CD3$^+$CD4$^+$FoxP3$^+$), DCs (CD11c$^+$), macrophages (CD11b$^+$F4/80$^+$), and neutrophils (CD11b$^+$Gr-1^{Hi}) (22). *B*, Heatmap of TrIP protein expression overlayed across the splenic populations. *C,* Quantification of TrIP MFI across each of the immune cell populations. *D,* Histograms depicting the range of TrIP expression in the indicated populations. *E,* Staining of WT vs TrIP knockout (*Pik3ip1$^{fl/fl}$E8i^{cre}*) CD8$^+$ T cells (CD3$^+$CD8$^+$) from naïve spleens. *F,* Gating strategy for naïve (CD62L$^+$) and antigen-experienced (CD44$^+$) CD8$^+$ T cells and corresponding TrIP expression. *G,* Quantification of TrIP-AF647 MFI in the CD8$^+$ T cell subpopulations, stratified by CD44 vs CD62L expression. *H,* Stimulation of whole WT P14 TCR Tg splenocytes with 200 ng/ml of WT gp33 peptide. TrIP and TCR Vα2 expression were followed over 24 hrs by flow cytometry. I, Quantification of TrIP expression MFI on CD8+ T cells in the 24 hrs following activation *in vitro*.

Kinetics of TrIP loss from activated T cells correlates with TCR signal strength

Existing data suggest that TrIP acts as a "rheostat" for initial PI3K and T cell activation downstream of the TCR. Therefore, we wanted to assess the relationship of TCR signal strength to the putative cleavage of TrIP after activation. We stimulated splenocytes from WT C57BL/6 mice with varying concentrations of plate-coated anti-CD3 plus anti-CD28 mAb's and used the 18E10 mAb to assay TrIP levels over time. We found that the kinetics of TrIP loss correlated with the strength of stimulation, in a roughly semi-logarithmic fashion (**Fig. 3A-B**). Next, we tested the relative contributions of signal 1 (TCR/CD3) and signal 2 (CD28 co-stimulation) on downregulation of TrIP following activation. To block CD28 co-stimulation, we pre-treated WT splenocytes with saturating amounts of CTLA4-Ig prior to stimulation with anti-CD3 mAb. These experiments suggested that the loss of TrIP does not require CD28 co-stimulation, as the degree and timing of TrIP downregulation were nearly identical with or without CD28 blockade (**Fig. 3C-D**).

To assess the sensitivity of TrIP loss to changes in TCR signal strength under more physiological conditions, we performed stimulation of T cells with antigen and antigen-presenting cells (APC). We thus stimulated splenocytes from P14 TCR Tg mice with cognate antigen (LCMV gp33 peptide presented by H-2D^{b}) and measured levels of cell surface TrIP on CD8^{+} P14 T cells over time, by flow cytometry. As shown in **Figure 3E**, we observed rapid and dramatic loss of cell-surface TrIP upon stimulation with gp33 peptide, similar to what we had observed after stimulation with anti-CD3 mAb. Importantly, this system also allowed us to test the effects of altered gp33 peptides with different affinities for the P14 TCR (23). Shown in **Figure 3E-F** are the results with two such peptides, with the higher affinity peptide (HiAff gp33) triggering the greatest degree of TrIP downregulation (>30%) by four hours after stimulation. By contrast, a lower affinity peptide (L6F gp33) caused very little TrIP loss after four hours (<5%). Thus, these data demonstrate that peptide/MHC affinity for the TCR is tightly linked with the kinetics of TrIP downregulation.

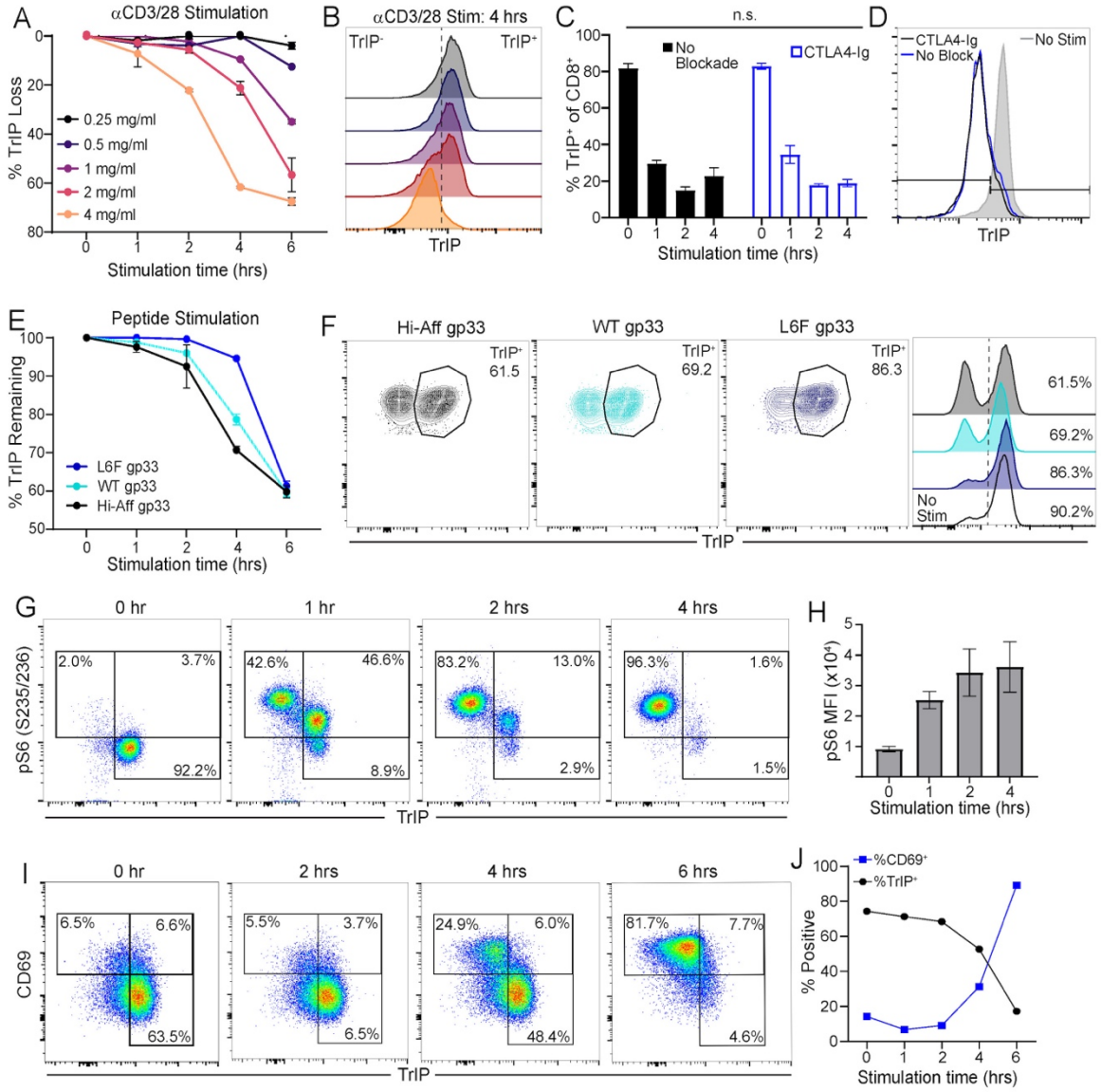

Figure 3. Stimulation strength-dependent downregulation of TrIP on CD8⁺ T cells. *A,* WT C57BL/6 splenocytes were stimulated with plate-coated anti-CD3 and anti-CD28 at the indicated concentrations and TrIP loss on the CD8⁺ T cells was followed over time by flow cytometry. *B,* Histogram of the TrIP expression on CD8⁺ T cells at the 4-hr timepoint of each dose. *C,* WT B6 splenocytes stimulated with 2 μg/ml of plate-coated anti-CD3 in the presence or absence of saturating amounts of CTLA4-Ig (20 μg/ml). *D,* Representative histogram overlay of CTLA4-Ig blockade experiment at the 1-hr timepoint. *E,* WT P14 TCR Tg splenocytes were stimulated with 100 ng/ml of the indicated cognate peptide variants (peptide affinity: Hi-Aff gp33>WT gp33>L6F gp33) and followed TrIP expression on the CD8⁺ T cells over time via flow cytometry. *F,* Representative TrIP staining of each peptide stimulation at the 4-hr timepoint, shown by both dot plot and histogram overlays. **G,** WT P14 splenocytes stimulated with 200 ng/ml of WT gp33 peptide showing staining for pS6(S235/S236) vs. TrIP staining in CD8⁺ T cells following activation. *H,* Quantification of pS6(S235/S236) MFI during the 4 hours of stimulation. *I,* CD69 vs TrIP expression from the same stimulation described in G-H. *J,* Frequencies of total TrIP⁺ and total CD69⁺ cells. Ordinary two-way ANOVA used for statistical comparisons (p: *<0.05, **<0.01, ***<0.001, ****<0.0001).

Although the functional relevance of acute cell-surface TrIP downregulation is not completely clear, such down-modulation of a negative regulator like TrIP may help to constrain early T cell activation, as suggested in previous publications from our group and others (16, 17). Consistent with this notion, we found that WT P14 CD8 T cells activated with cognate peptide seem to progress through three distinct stages of early T cell activation, distinguished by their relative expression of TrIP and phosphorylation of the S6 ribosomal subunit (pS6) (**Fig. 3G**). Starting with a naïve (i.e. $TrIP^+$) population of $CD8^+$ T cells, we found that after one hour of stimulation with 200 ng/ml of WT gp33 peptide, a small proportion (<10%) of the cells had yet to undergo activation, indicated by a lack of pS6 staining. Somewhat unexpectedly, we found a distinct population of pS6-intermediate ($pS6^{int}$) cells which still maintained their TrIP expression. This intermediate pS6 intensity is consistent with the regulatory activity that TrIP plays during early T cell activation, as loss of TrIP coincides with a secondary increase in pS6 signal intensity that then persists beyond four hours of stimulation (**Fig. 3H**). These data further suggest that the loss of TrIP is not a pre-requisite for active PI3K signaling, but rather may act to modulate PI3K signal intensity at the early stages of CD8 T cell activation. To provide additional functional context to TrIP expression following T cell activation, we assessed whether there was a temporal association between TrIP downregulation and expression of a well-established early indicator of T cell activation, CD69. As shown in **Figure 3I**, we did in fact observe a tightly associated inverse correlation between loss of cell-surface TrIP and expression of CD69 (**Fig. 3J**).

Role of TCR-dependent signaling pathways in acute TrIP protein loss

Next, we sought to better understand which specific TCR signaling pathways regulate TrIP surface expression. Initially, we hypothesize that PI3K signaling itself might act in a feed-forward loop, directly leading to TrIP downregulation. To investigate this, we took a pharmacological approach, using well-defined inhibitors to target various PI3K pathway members, including PI3K itself (IC87114), Akt (MK2206), and mTORC1 (rapamycin). Using WT P14 splenocytes with gp33

peptide stimulation, as above, we pre-treated cells with the indicated inhibitors for 30 minutes prior to the addition of WT gp33 peptide. As shown in **Figure 4A**, we found that regardless of which PI3K pathway member was targeted for inhibition, each was able to preserve only a modest, although statistically significant, amount of TrIP expression during two hours of stimulation (**Fig. 4B**). As expected, we also observed lower pS6 staining in each of the drug treated samples compared to the untreated control (**Fig. 4C-D**), confirming the effectiveness of the inhibitors. It is important to note that enhanced persistence of TrIP expression by inhibitor treatment may have exacerbated the suppression of pS6 signals we observed when comparing to the untreated control. These data suggest that while modulating the PI3K pathway can lead to small differences in TrIP expression, this pathway does not appear to play a major role in the surface level downregulation following TCR activation.

We next expanded the scope of these experiments to include inhibitors targeting a broader range of pathways. This included inhibitors of calcium signaling (FK-506; a calcineurin inhibitor), ERK (U0126; MEK1/2 inhibitor), and finally dasatinib (a Src family kinase inhibitor). Perhaps unsurprisingly, the potent inhibition of upstream kinases by dasatinib (which would include Lck) resulted in broad inhibition of TCR signaling and significant preservation of TrIP expression (>50%) at two hours after stimulation (**Fig. 4E-F**). Although, importantly, dasatinib treatment did not wholly prevent T cell activation and TrIP loss, as we still observed complete TrIP loss at the four-hour timepoint, similar to the no-drug group (**Fig. 4E-F**). Moving further downstream of the TCR, we found that inhibition of either calcineurin or MEK1/2 activity under these conditions also led to significant preservation of TrIP expression (at least 60% and 40% of starting levels, respectively) in $CD8^+$ T cells following two hours of stimulation, compared to around eighteen perecent in the untreated control (**Fig. 4E-F**). While these inhibitors showed much more potent prevention of TrIP downregulation following two hours of activation than what was observed with the PI3K inhibitors, the effects were transient and TrIP expression was almost completely lost by four hours in all cases (**Fig. 4F**). These data suggest that downregulation of TrIP surface

expression following TCR/activation is likely not directly controlled by a direct PI3K-mediated negative feedback loop. Rather, our results show that calcium and ERK-MAPK signaling play more direct roles.

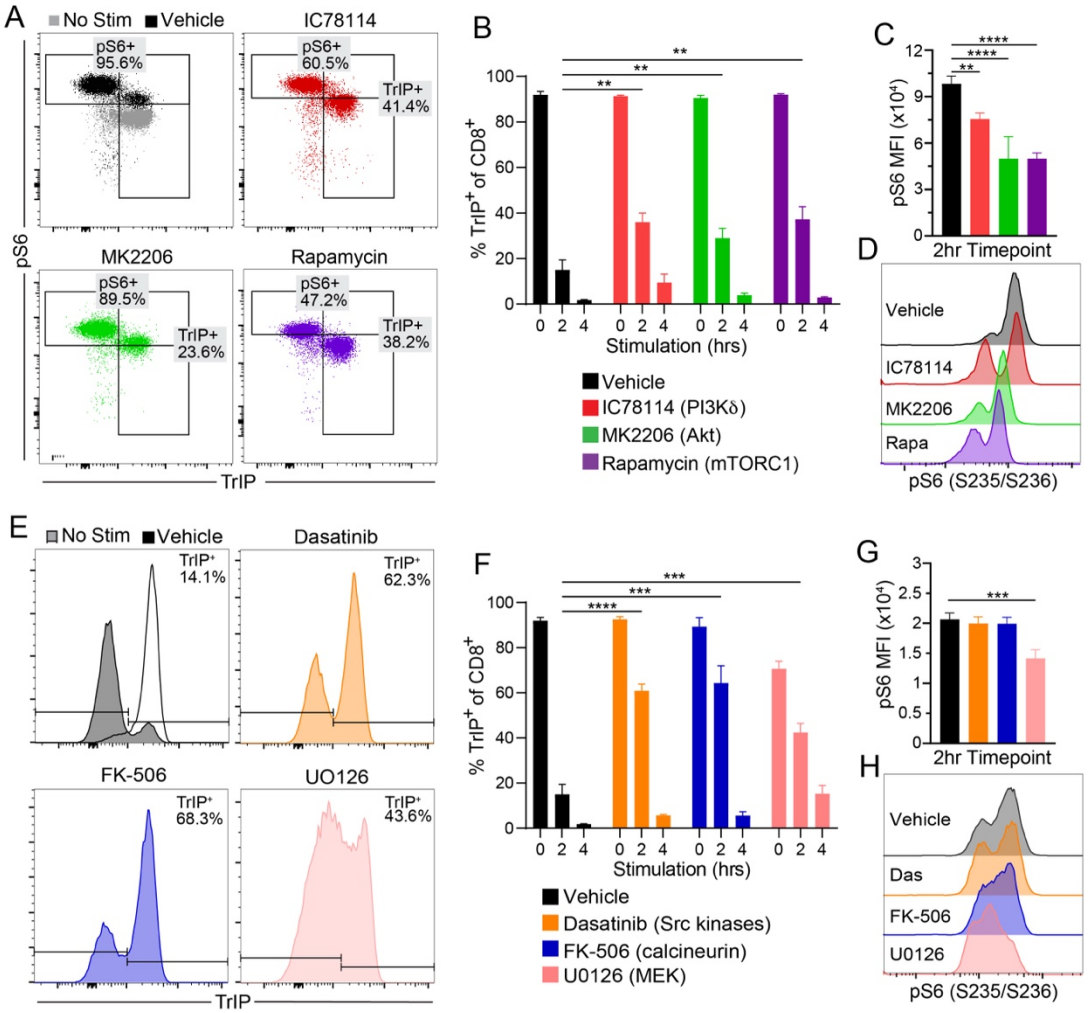

Figure 4. The PI3K pathway is dispensable for TrIP downregulation. WT P14 splenocytes were pre-treated for 30 minutes with the indicated inhibitors and then stimulated with 200 ng/ml cognate WT gp33 peptide maintaining inhibition throughout the stimulation. TrIP loss on the CD8$^+$ T cells was followed over time by flow cytometry. *A,* Dot plots showing pS6(S235/S236) vs TrIP expression on the CD8$^+$ T cells at the 2-hr timepoint. *B,* Quantification of TrIP expression at each timepoint for each treatment *C,* Quantification of pS6(S235/S236) MFI at the 2-hr timepoint. *D,* Representative histograms of pS6(S235/S236) staining at the 2-hr timepoint. *E,* Representative histograms of TrIP expression at the 2-hr timepoint following stimulation. *F,* Quantified summary of TrIP expression at each timepoint for each treatment. *G,* Quantification of pS6 levels at the 2-hr timepoint. *H,* Representative histograms of pS6 staining at the 2-hr timepoint. Ordinary two-way ANOVA was applied for statistical comparisons (where p: *<0.05, **<0.01, ***<0.001, ****<0.0001).

In addition to calcium (Ca^{2+}) and PIP_3, another critical second messenger downstream of TCR signaling is diacylglycerol (DAG), which functions in part to activate several isoforms of protein kinase C (PKC). The PKC family of serine/threonine kinases comprises three major classes based on their physiological activators. The classical PKCs (α, βI, βII, and γ) and the novel PKCs (δ, ε, η, and θ) both require diacylglycerol (DAG) for activation, but while the classical PKCs also require Ca^{2+} the novel PKCs do not (24). By contrast, so-called atypical PKCs (ζ and λ/ι) require neither DAG nor Ca^{2+} for activation (24). Since PKCs are connected to both calcium and ERK signaling, we hypothesized that one or more PKC family members may play a key role in regulating TrIP downregulation. To address this, we employed multiple inhibitors targeting a broad range of PKCs. Bisindolylmaleimide I (Bis I) was used to inhibit the classical PKCs; sotrastaurin and Gö6983 are both pan-PKC inhibitors which have specificities for both the classical and novel PKC. Thus, these PKC inhibitors nearly completely prevented TrIP loss from P14 T cells after two hours of stimulation, whereas the untreated condition showed over 55% TrIP loss from baseline (**Fig. 5A-B**). Despite the persistence of TrIP expression upon treatment with these inhibitors, we found that the cells were still able to upregulate pS6(235/236) (**Fig. 5C-D**), albeit to a lower degree compared to control. Interestingly, we found that the inhibitors sotrastaurin and Gö6983, which target both classical (α, βI, βII, and γ) and the novel PKCs (δ, ε, η, and θ), both were able to preserve TrIP expression for the first two hours of activation, but the effects faded by the four-hour timepoint (**Fig. 5B**). This is in contrast to more specifically inhibiting the classical PKCs with Bis I, where we were surprised to observe not only the persistence, but a notable increase, in TrIP expression two hours after activation (**Fig. 5B**). Furthermore, this expression was only subtly decreased even following four hours of stimulation in the Bis I treated cells. These data suggest that PKCs play a major role in regulating the surface downregulation of TrIP following TCR stimulation, and that the classical PKCs may play a larger role in this process.

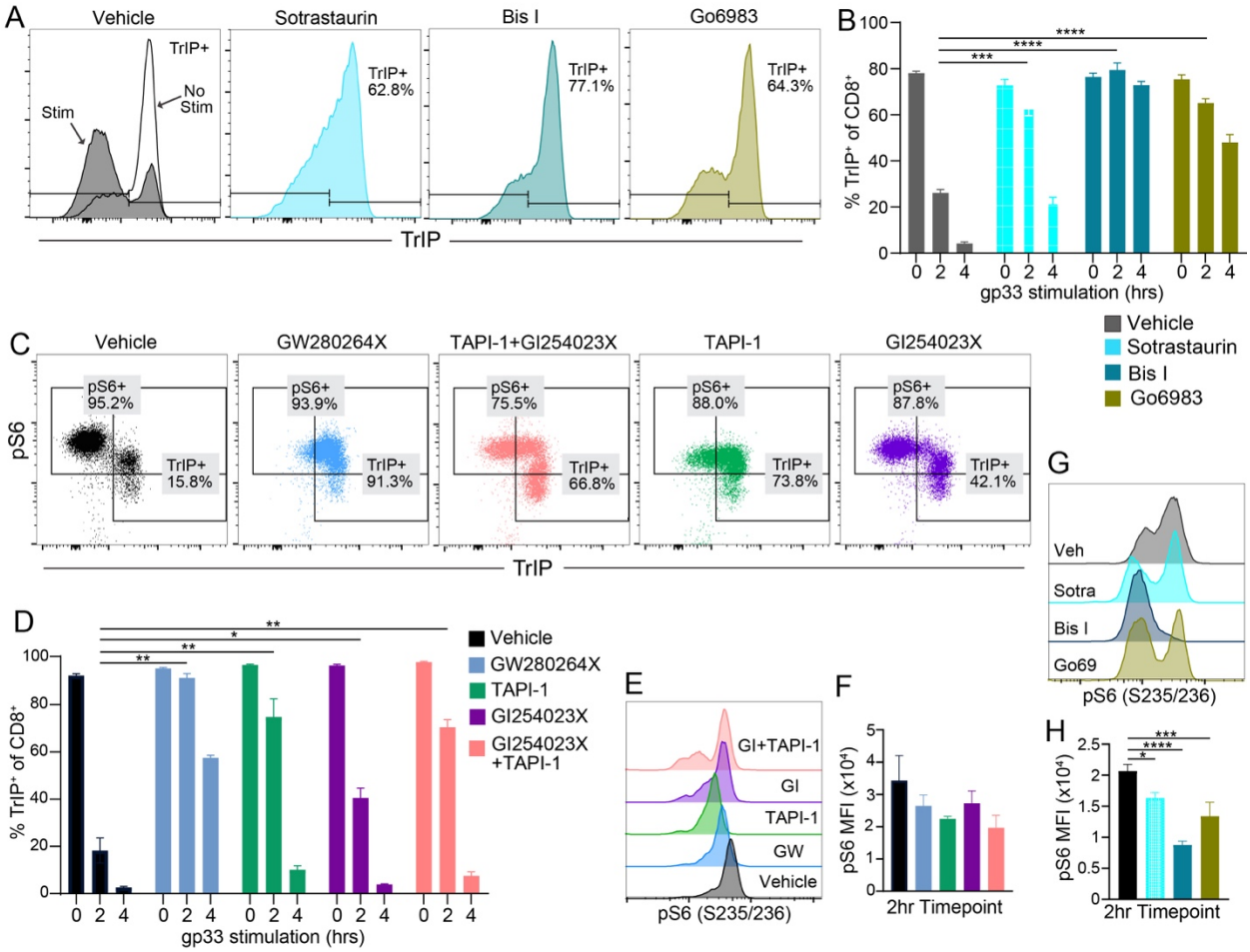

Figure 5. PKC and ADAM17 activity are required for downregulation of cell-surface TrIP. WT P14 splenocytes were stimulated with 200 ng/ml WT gp33 peptide in the presence of the indicated inhibitors. TrIP loss on the CD8$^+$ T cells was followed over time by flow cytometry. *A,* Flow plots of TrIP staining in each PKC inhibitor treatment at 2-hr timepoint following stimulation. *B,* Quantification of TrIP expression at each timepoint for each PKC inhibitor treatment. *C,* Representative histograms of pS6(S235/S236) staining at the 2-hr timepoint. *D,* Quantification of pS6(S235/S236) MFI at the 2-hr timepoint. *E,* Representative flow plots pS6(S235/S236) vs TrIP expression treatment at the 2-hr timepoint in the presence of ADAM inhibitors. *F,* Quantification of TrIP expression across each ADAM inhibitor treatment. *G*, Representative histograms of pS6(S235/S236) staining at the 2-hr timepoint. *H,* Quantification of pS6(S235/S236) MFI at the 2-hr timepoint. Two-way ANOVA statistical analysis applied for statical comparison (where p: *<0.05, **<0.01, ***<0.001, ****<0.0001).

Role of metalloproteases in acute TrIP downregulation

While the above data further define the cellular signaling pre-requisites for TrIP downregulation, we have yet to fully understand the direct mechanism by which TrIP is lost. Shedding of surface proteins by proteolytic cleavage has been shown to play numerous immunological roles, with the ADAM (A disintegrin and metalloproteinase domain-containing) family of proteases playing

prominent roles (25–27). In fact, our initial studies using expression of Flag-tagged TrIP in T cell lines (16) revealed that the inhibitor GW280264X (a dual inhibitor of ADAM10/ADAM17) prevented stimulation-induced downregulation of TrIP (16). Thus, we wanted to evaluate if endogenous murine TrIP operates in a similar manner. Utilizing the same P14 TCR/gp33 peptide stimulation system as above, we used GI254023X and TAPI-1, to inhibit ADAM10 or ADAM17 (aka TNF-α converting enzyme or TACE), respectively, as well as employing the dual inhibitor GW280264X. As shown in **Figure 5E-F**, we found that inhibition of both ADAM10/17 (using GW289264X) resulted in significant preservation of TrIP expression following stimulation. When targeting ADAM10 or ADAM17 separately, we observed a greater effect with the specific ADAM17 inhibitor (TAPI-1), compared to the ADAM10 inhibitor (GI2540230X), suggesting a greater role for the former in TrIP downregulation during T cell activation. Prevention of TrIP downregulation also corresponded with lower levels of pS6 induction (**Fig. 5G-H**), indicative of TrIP inhibition. Confirming a major role for ADAM17, we found that combining GI254023X and TAPI-1 was only sufficient to match the levels of TrIP preservation seen in the TAPI-1 only condition (**Fig 5E-F**). In fact, although we refer to GI254023X as an ADAM10 inhibitor for these studies it still has some cross-reactivity to ADAM17, albeit with 100-fold lower potency, thus its more moderate effects may be attributed to its effect on ADAM17 independent of ADAM10. Together, these data suggest that surface downregulation of TrIP occurs via metalloprotease-mediated cleavage, primarily carried out by ADAM17.

Structural requirements for TrIP downregulation

Next, we wanted to understand where in the ecto domain of TrIP the ADAM-mediated cleavage occurs. We focused on the 76-amino acid long connecting “stalk domain” linking the extracellular kringle domain to the transmembrane and intracellular domains (**Fig. 6A**). Assessment of the putative structure of this protein in AlphaFold (28, 29) suggests that the extracellular ‘stalk domain’ region of TrIP is likely unstructured in nature (**Fig. 6A**). Initially, we explored *in silico* prediction

methods (e.g. iProt-Sub) to identify predicted metalloprotease cleavage sites (30). While producing multiple possible sites, they spanned a wide range up and down the extracellular 'stalk domain' (**Fig. 6A**), and thus did little to narrow down the region(s) where cleavage might occur. The shortcomings of these types of prediction are likely due to the somewhat promiscuous cleavage specificity of ADAM17 (31, 32). Reports suggest that ADAM17 cleavage typically occurs in sites proximal to the cell membrane (33), so we focused on that area of the TrIP protein. Thus, we made a series of internal deletion mutants to both help confirm that cleavage is indeed the mechanism by which cell-surface TrIP is downregulated and to create a non-cleavable TrIP construct for future functional studies. The sites of these deletions are indicated in **Figure 6B**; each construct also included a Flag-tag for specific detection.

Next, we transfected D10 T cells with the constructs encoding either FL TrIP or each of the truncations mutants described above, and assessed stability of the proteins after stimulation with antibodies to CD3 and CD28 or with PMA and ionomycin. We also assessed PI3K pathway signaling by tracking S6 phosphorylation in the stimulated cells. Thus, we found that when we stimulated D10 T cells expressing either FL TrIP or the 16aa deletion, the extent and kinetics of TrIP downregulation were indistinguishable (**Fig. 6D-E, G**). By contrast, however, there was no detectable downregulation of the TrIP construct with the 29aa deletion following stimulation, even when cells were stimulated with PMI plus ionomycin (**Fig. 6F-G**). In addition, we observed significantly higher baseline expression of the 29aa deletion construct, compared with WT TrIP and the 16aa deletion (**Fig. 6G**). It is still unclear whether this is due to enhanced translation or processing of the transfected protein or whether it might be the result of diminished steady-state cleavage of TrIP. Consistent with our previous study (16) and data shown above, expression of a cleavage-resistant form of TrIP led to a decrease in pS6 staining in D10 T cells transfected with 29aa deletion construct, compared with cells expressing either the FL or 16aa form (**Fig. 6H**). Together, these data expand our understanding of TrIP regulation in a non-reductionist manner, showing that TrIP cleavage from the surface by ADAM17 (TACE) occurs in the stalk, possibly

between residues 120 and 133, and that in the absence of TrIP downregulation, partial suppression of the PI3K/Akt pathway is maintained.

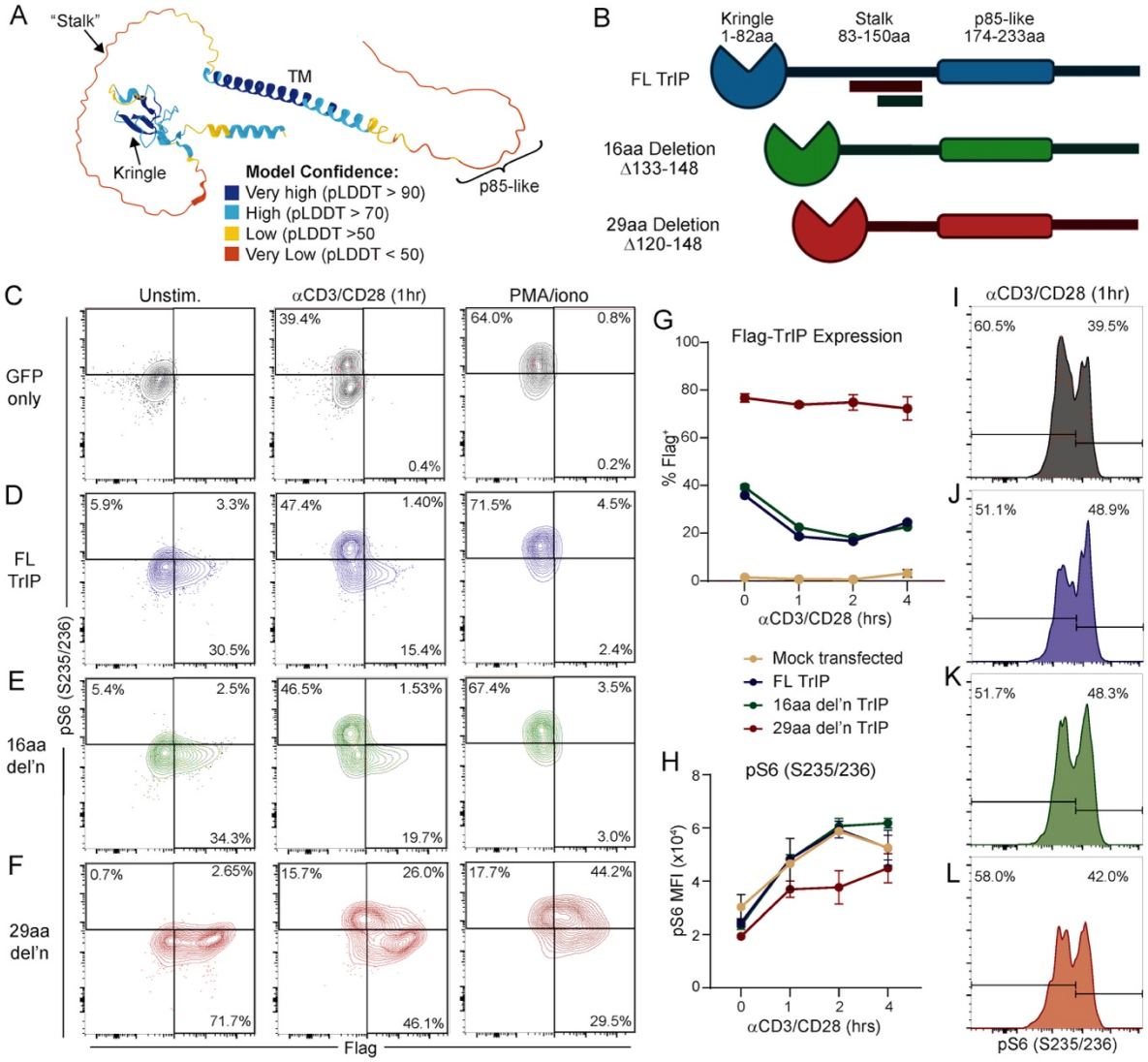

Figure 6: Truncation of the extracellular stalk renders TrIP resistant to cleavage and dampens PI3K signaling. D10 T cells were co-transfected with pMaxGFP alone or together with the indicated TrIP plasmid constucts. Twenty four hours following transfection, cells were stimulated with 10 μg/ml plate-coated anti-CD3 + anti-CD28 or PMA/ionomycin (50 ng/mL and 500 ng/mL, respectively). *A,* AlphaFold-computed predicted crystal structure of TrIP protein, indicated is the model confidence by color. *B,* Diagram depecting the two truncation mutants used in these studies. All flow plots show cells gated on GFP$^+$, *C-F,* D10 T cells were transfected with GFP control alone (C) or together with FL TrIP (D) or the 16aa (E) or 29aa (F) deletions of TrIP. The next day, cells were stimulated as indicated at the top of each column, for one hour, and cells were stained with antibodies to Flag and pS6 (S235/S236). Contour plots are based on gating of GFP+ cells. *G,* Quantification of ther percentage of Flag+ cells in the transfected D10 cells following αCD3/CD28 stimulation. *H,* Quantification of pS6(235/236) MFI in transfected cells after αCD3/CD28 stimulation.

Discussion

In this study, we expand on the understanding of TrIP, a transmembrane protein comprised of an extracellular protein-protein interaction kringle domain (34, 35), and an intracellular 'p85-like' domain (15, 16, 18). The p85-like domain of TrIP has been shown to interact with the p85/p110 heterodimer of PI3K and negatively regulate its catalytic activity, although this is not a complete inhibition (18). Furthermore, expression of TrIP in T cells has been shown to negatively regulate their activation and that its deletion can enhance their inflammatory activities (15, 16). While gaining valuable insight into fundamental TrIP biology, these previous studies were hindered by the absence of a commercially available anti-murine TrIP monoclonal antibody and thus relied on cell line expression systems and knockouts to characterize its function. In this study, we describe the production and validation of three novel anti-mTrIP IgG monoclonal antibodies capable of recognizing endogenous murine TrIP protein for detection by flow cytometry. Each of the three clones appears to stain TrIP via its kringle domain, since deletion of that domain completely abrogated their staining. Consistent with the high sequence homology (>80%) between mouse and human TrIP, we did observe some cross-reactivity of human TrIP by the 18E10 clone. However, this was significantly weaker than its reactivity with murine TrIP, since staining was only detectable when using a secondary antibody. Thus, future translational studies will likely require generation of more robust antibodies specific to human TrIP.

Consistent with publicly accessible gene expression data, splenic T and B lymphocytes demonstrated some of the highest levels of TrIP protein expression. Nonetheless, we also observed relatively high expression of TrIP on neutrophils, something that has not yet been reported in the literature. Furthermore, upon subsetting the CD8 T cells based on their CD44 vs. CD62L expression, we found that the naïve CD62L$^+$ cells comprise the majority of the TrIP-expressing cells, whereas it was not detectable on CD44$^+$ cells. We further showed that this endogenous TrIP expression on naïve CD8$^+$ T cells is lost within the first few hours after TCR stimulation, confirming our previous studies with the D10 helper T cell line (16). Building upon

these data, we found that TrIP expression is lost following stimulation with anti- CD3 mAb or peptide antigen in a dose-dependent manner. Furthermore, this loss appears to be largely independent of the “signal 2” (CD28) contribution, as blockade with CTLA4-Ig had little-to-no effect. While having confirmed previous studies that suggested TrIP expression would be found on naïve T cell populations and lost upon activation, it was unclear when, or even if, TrIP may be re-expressed following T cell activation. Our results show that although TrIP expression does remain low for up to twelve hours following activation, some cells do begin to re-express TrIP by 24 hours, at least *in vitro*. This re-expression of TrIP suggests it may play a previously unexplored role in longer lived populations like memory T cells, a subject that is worthy of further study.

The ability to track endogenous TrIP protein on T cells has given us a new understanding of how TrIP expression may coordinate early T cell activation signals. Ours is the first study, that we know of, to describe an early activation state in $CD8^+$ T cells during which TrIP is still expressed and there is an intermediate level of PI3K activation (as read-out by pS6). This temporally correlated series of signaling events adds to our understanding of the complex role of TrIP in early T cell activation. Along with the kinetics of S6 phosphorylation, we also found that upregulation of CD69, a well-characterized marker of early T cell activation (36), was inversely correlated with the downregulation of TrIP.

We also conducted a thorough study of the relationship of TrIP downregulation to TCR signaling pathways through the use of pharmacological inhibitors. First, we targeted various members of the PI3K pathway, but these inhibitors had little effect on the kinetics of TrIP downregulation. These data suggest that the PI3K pathway itself does not play a role in downregulation of TrIP. Expanding our investigations to other pathways, we found that the inhibition of either calcium signaling (via calcineurin inhibition) or ERK activity (via MEK1/2 inhibition) had a much more significant impact on TrIP expression following activation. These data led us to investigation the role of the protein kinase C (PKC) family of enzymes, as some members of this family are activated in a Ca^{2+}-dependent manner and are generally known to promote

activation of MAPK signaling (26, 37). We found that broad inhibition of PKC activity significantly preserves the expression of TrIP following T cell activation. Consistent with reports showing that novel PKC isoforms are required for ADAM17-mediated cleavage, inhibition of ADAM17 completely abrogated TrIP loss (dependent on drug potency), while ADAM10 did not appear to play a role in this process.

Further investigation of TrIP downregulation revealed that the apparently ADAM17-mediated cleavage occurs within a 29 amino acid region of the extracellular domain, since removal of this segment could completely prevent downregulation. Nonetheless, we cannot conclusively state that we have removed the site of cleavage. Thus, it is formally possible that the shortening of the protein by 29 amino acids may lead to hindrance of ADAM17 access to the stalk domain, thereby sterically preventing cleavage of TrIP. Interestingly, we also found that the non-cleaveable version of TrIP displayed higher baseline expression, compared to WT constructs, implying that TrIP is subject to low rates of basal shedding, even in the absence of TCR stimulation. Further investigations are needed to fully elucidate the specific cleavage site and what impact the constant expression and low level shedding of TrIP would have on T cell activation and differentiation.

Finally, we present data expanding our understanding of the relationship of TrIP expression to signals that regulate T cell activation. Thus, we found that TrIP downregulation occurs in a TCR signal strength-dependent manner, suggesting it may play a previously undescribed role in controling early T cell response to low levels of antigen. Supporting these data, we found a seemingly step-wise progression of T cell activation demarcated by persisting TrIP expression early on during stimulation whose subsequent removal leads to maximal T cell signaling and activation. Future studies on the downstream effects of TrIP loss in specific disease contexts are still needed to fully understand the impact of TrIP regulation in the T cell compartment.

Experimental Procedures

Antibodies and flow cytometry

For extracellular staining, single cell suspensions were stained at 4°C for 30 minutes with Live/Dead + antibody cocktail containing anti-CD16/CD32(Fc Shield) (Tonbo Biosciences: clone 2.4G2) resuspended in PBS. For intracellular staining, cells were fixed/permeabilized using the eBioscience Foxp3/Transcription factor staining buffer set (00-5523-00), as per manufacturer instructions. Following fixation, Intracellular staining antibodies were resuspended in 1x permeabilization buffer and used to stain at 4°C for 30 minutes.

The following antibodies and dyes were used for these analysies; anti-CD90.2 (BD Biosciences: clone 53-2.1), anti-CD8α (BD Bioscience: clone 53-6.7), anti-CD44 (BD Biosciences: clone IM7), anti-CD11c (BD Biosciences; clone N418), anti-TCRβ (BD Biosciences: clone H57-597), anti-CD4 (Biolegend: clone RM4-5), anti-CD11b (ThermoFisher: clone M170), anti-CD62L (Biolegend: clone MEL-14), anti-F4/80 (Biolegend: clone BM8), anti-CD25 (BD Biosciences: clone 7D4), anti-Gr-1 (Invitrogen: clone RB6-8C5), anti-CD19 (Biolegend: clone 1D3), anti-Foxp3 (Invitrogen: FJK-16s), anti-pS6(235/236) (Cell Signaling: clone D57.2.2E), anti-TCR Vα2 (Biolegend: clone AF-7), anti-CD69 (Biolegend: clone H1.2F3), anti-Flag (Biolegend: clone L5). Live/dead staining was done using the Zombie NIR fixable viability kit (BioLegend, 423105).

For the majority of TrIP staining studies, the 18E10 clone showed the most robust and reproducable staining and therefore was the monoclonal used for the endogenous murine TrIP studies. We directly conjugated the TrIP-18E10 to Alexa Fluor 647 using a commercial labeling kit (Invitrogen Alexa Fluor 647 Antibody Labeling Kit; A20186), per manufacturers instructions. All flow cytometry was preformed on a 5-laser Cytek Aurora and flow cytometry data were analyzed with FlowJo (v10.10.0).

Mice

We previously generated a conditional mouse knockout strain where LoxP sites were inserted into the TrIP gene (*Pik3ip1*$^{fl/fl}$), targeting the removal of exons 2-5 (16). We then crossed these to E8i^{cre} mice (originally from Jackson; Strain #008766), whereby Cre-mediated recombinase will result in splicing and removal of exons 2-5 of the *Pik3ip1* gene specifically in CD8^{+} T cells. For peptide stimulation studies, we employed the P14 TCR transgenic strain that carries a re-arranged T cell receptor specific for the gp33 peptide from LCMV (Jackson; Strain # 037394). All strains were backcrossed more than 9 generations to C57BL/6J (Jackson; Strain #000664). All mice were bred in-house under SPF conditions, and experimental mice were either littermates or housed in the same facility and same room. All experiments were conducted on mice 6-8 weeks of age, with age and sex-matched groups. All animal procedures were conducted in accordance with NIH and University of Pittsburgh IACUC guidelines.

Generation of TrIP-Ig fusion protein

To generate the TrIP-Ig fusion, the ecto domain of murine TrIP/Pik3ip1 was PCR amplified from IMAGE consortium clone number 4039129, using primers to add EcoRV and BglII sites at the 5' and 3' ends, respectively. This fragment was then cloned into the same restriction sites of pFuse-hIgG1-Fc2. Reading frame and integrity of the cloned fragment were confirmed by sequencing. This plasmid was then transfected into HEK293T cells and Protein-A purified by a commercial vendor (SydLabs, Inc.).

Development of mAb's to the ecto domain of TrIP

Monclonal antibodies to the ecto domain of murine TrIP were developed in conjunction with a commercial vendor (Rockland, Inc.). Briefly, Sprague-Dawley rats were immunized with the aforementioned TrIP-Ig fusion protein. Immunized rat splenocytes were then fused with Sp2/0-

Ag14 myeloma cells to generate hybridomas. These hybridomas were subsequently subcloned one or more generations via limiting dilution. Reactivity/specificity of each was initially screened via ELISA for reactivity with recombinant TrIP-Ig protein, and counter-screened against human IgG1.

Generation of TrIP deletion mutant constructs

For the initial antibody validation experiments, full-length human *PIK3IP1* and full-length mouse *Pik3ip1* gBlocks (IDT) were cloned into the pcDNA3.1 expression vector via restriction enzyme cloning. For TrIP cleavage experiments, two truncated and one full-length TrIP gBlocks (IDT) were produced and cloned via restriction enzyme cloning into a minimal pcDNA3.1(+) backbone modified from a commercial pcDNA3.1(+) expression construct (Invitrogen). In the first TrIP truncation, a 16 amino acid sequence was removed [AA positions 133-148; (DNA sequence: CAGTCAGCTTGTGAGGATGAACTCCAAGGAAAAAAAAGACCTAGGAAC)]. For the second truncated TrIP construct, we extended that deletion an additional 13 amino acids to make a 29 amino acid deletion construct [AA positions 120-148 removed; (DNA sequence: AGGAGTGAGGCAGCCGAGGTGCAGCCAGTGATCGGGATCAGTCAGCTTGTGAGGATGAA CTCCAAGGAAAAAAAAGACCTAGGAAC)]. Each plasmid construct used for transfections was designed to include a Flag tag (an 8 amino acid sequence: DYKDDDDK) for antibody recognition via anti-Flag antibody (clone: L5). All plasmid constructs' MCS were verified by Sanger sequencing.

Cell lines, transfections and activation

Human embryonic kidney (HEK) 293T cells were cultured in DMEM containing 10% BGS, 1% penicillin/streptomycin, and 1% L-glutamine. D10.G4.1 mouse T helper cell line (D10 cells) were maintained in 50-units/ml rhIL-2 in complete RPMI (cRPMI) media (cRPMI supplemented with 10% BGS, 1% penicillin/streptomycin, 1% L-glutamine, 0.05 mM 2-mercaptoethanol, 1x non-

essential amino acids, 1% HEPES, and 1% sodium pryuvate). Transfections of HEK293T cells was done using TransIT-LT1 (Mirus Bio; MIR 2304) per manufacturer instructions. Transfection of D10 cells via electroporation was done using a Bio-Rad GenePulser Xcell (Square Pulse protocol; 400V, 3 pulses, 0.5 ms pulse length, 0.05 s between pulses). For truncated TrIP expression experiments, pMaxGFP was co-transfected as a positive control (Lonza Biosciences). Activation of D10 cells was done via plate-coated anti-CD3 (clone:145-2C11; Tonbo Biosciences 50-201-4837); anti-CD28, (clone 37.51; Biolegend: 102101).

Mouse Tissue Processing and *In Vitro* Stimulation

Spleens harvested from either WT C57BL/6J or WT P14 TCR Tg mice were mechanically disrupted and filtered to single cell suspensions. Red blood cells were removed via 1x RBC lysis buffer (eBioscience,00-4333-57), according to manufacturer instructions. Splenocyte stimulations were done in complete RPMI (cRPMI) media (cRPMI supplemented with 10% BGS, 1% penicillin/streptomycin, 1% L-glutamine, 0.05 mM 2-mercaptoethanol, 1x NonEessential Amino Acids, 1% HEPES, and 1% sodium pryuvate). Anti-CD3 (clone:145-2C11; Tonbo Biosciences 50-201-4837); and anti-mCD28, clone 37.51; Biolegend: 102101) were used for plate-coating at the indicated concentrations. For P14 TCR Tg stimulations, three different peptides were selected based on published work by J. M. Boulter *et al*. (23); a high affinitiy gp33 peptide (sequence: KAVYNFATM), the WT gp33 peptide (sequence: KAVYNFATC), and a peptide with lower affinity L6F gp33 (sequence: KAVYNLATC).

Inhibitors

For the *in vitro* TrIP downregulation experiments, inhibitors used were as follows: IC87114 (SellickChem; S1268), 10 μM; MK-2206 (Cayman Chem; 11593), 2.5 μM; rapamycin (SellickChem; S1039), 100 nM; dasatinib (Stemcell; 73082), 2.5 nM; FK-506 (SellickChem; S5003), 10 μM. U0126 (MedChemExpress; HY-12031), 2.5uM; bisindolylmaleimide I

(SellickChem; S7208), 10 μM; sotrastaurin (SellickChem; S279101), 5 μM; Go6983 (MedChemExpress; HY-13689), 2.5 μM; GW280264X (Bio-Techne; Cat# 7030), 1μM; GI254023X (Selleckchem; S8660), 5μM, TAPI-I (Selleckchem; S7434) 5μM. Cells were pre-treated with inhibitor for 30 minutes prior to peptide stimulation, with the inhibitor present at the indicated final concentrations throughout the stimulation.

Data Availability Statement

All data are contained in the manuscript.

Acknowledgements

This work was supported by grants from the NIH (F31CA261039 and T32CA082084 to B.M.) and (R01 GM136148 to L.P.K.). We would like to thank Grace Bowman and Edgar Cardona for their help with our mouse genotyping. We would also like to thank the Unified Flow Cytometry Core.

Author Contributions

B.M., S.R., H.B., and L.P.K. contributed to conceptualization. Funding acquisition contributed by B.M. and L.P.K., Data curation, formal analysis, and validation were performed by B.M., S.R., and U.U. Experiments were performed by B.M., S.R., H.B., L.L., U.U., and A.W. Writing – original draft by B.M., Supervision and manuscript editing were performed by L.P.K.

Conflict of Interest

The authors declare that they have no conflicts of interest relevant to the contents of this article.

References

1. Toker, A. (2002) Phosphoinositides and signal transduction. *Cell. Mol. Life Sci.* **59**, 761–779

2. Kapeller, R., and Cantley, L. C. (1994) Phosphatidylinositol 3-kinase. *Bioessays*. **16**, 565–576

3. Anderson, R. A., Boronenkov, I. V., Doughman, S. D., Kunz, J., and Loijens, J. C. (1999) Phosphatidylinositol phosphate kinases, a multifaceted family of signaling enzymes. *J. Biol. Chem.* **274**, 9907–9910

4. Madsen, R. R., and Vanhaesebroeck, B. (2020) Cracking the context-specific PI3K signaling code. *Sci. Signal.* 10.1126/scisignal.aay2940

5. Okkenhaug, K., Turner, M., and Gold, M. R. (2014) PI3K Signaling in B Cell and T Cell Biology. *Front. Immunol.* **5**, 557

6. Fruman, D. A., and Bismuth, G. (2009) Fine tuning the immune response with PI3K. *Immunol. Rev.* **228**, 253–272

7. Murter, B., and Kane, L. P. (2020) Control of T lymphocyte fate decisions by PI3K signaling. *F1000Res.* 10.12688/f1000research.26928.1

8. Ward, S. G., and Cantrell, D. A. (2001) Phosphoinositide 3-kinases in T lymphocyte activation. **13**, 332–8.

9. Zambricki, E., Shigeoka, A., Kishimoto, H., Sprent, J., Burakoff, S., Carpenter, C., Milford, E., and McKay, D. (2005) Signaling T-cell survival and death by IL-2 and IL-15. *Am. J. Transplant.* **5**, 2623–2631

10. Srivastava, N., Sudan, R., and Kerr, W. G. (2013) Role of inositol poly-phosphatases and their targets in T cell biology. *Front. Immunol.* **4**, 288

11. Fruman, D. A., Chiu, H., Hopkins, B. D., Bagrodia, S., Cantley, L. C., and Abraham, R. T. (2017) The PI3K pathway in human disease. *Cell*. **170**, 605–635

12. Lucas, C. L., Chandra, A., Nejentsev, S., Condliffe, A. M., and Okkenhaug, K. (2016) PI3Kδ and primary immunodeficiencies. *Nat. Rev. Immunol.* **16**, 702–714

13. Preite, S., Gomez-Rodriguez, J., Cannons, J. L., and Schwartzberg, P. L. (2019) T and B-cell signaling in activated PI3K delta syndrome: From immunodeficiency to autoimmunity. *Immunol. Rev.* **291**, 154–173

14. Andreotti, A. H., Schwartzberg, P. L., Joseph, R. E., and Berg, L. J. (2010) T-cell signaling regulated by the Tec family kinase, Itk. *Cold Spring Harb. Perspect. Biol.* **2**, a002287

15. DeFrances, M. C., Debelius, D. R., Cheng, J., and Kane, L. P. (2012) Inhibition of T-cell activation by PIK3IP1. *Eur. J. Immunol.* **42**, 2754–2759

16. Uche, U. U., Piccirillo, A. R., Kataoka, S., Grebinoski, S. J., D'Cruz, L. M., and Kane, L. P. (2018) PIK3IP1/TrIP restricts activation of T cells through inhibition of PI3K/Akt. *J. Exp. Med.* **215**, 3165–3179

17. Chen, Y., Wang, J., Wang, X., Li, X., Song, J., Fang, J., Liu, X., Liu, T., Wang, D., Li, Q., Wen, S., Ma, D., Xia, J., Luo, L., Zheng, S. G., Cui, J., Zeng, G., Chen, L., Cheng, B., and Wang, Z. (2019) Pik3ip1 Is a Negative Immune Regulator that Inhibits Antitumor T-Cell Immunity. *Clin. Cancer Res.* **25**, 6180–6194

18. Zhu, Z., He, X., Johnson, C., Stoops, J., Eaker, A. E., Stoffer, D. S., Bell, A., Zarnegar, R., and DeFrances, M. C. (2007) PI3K is negatively regulated by PIK3IP1, a novel p110 interacting protein. *Biochem. Biophys. Res. Commun.* **358**, 66–72

19. Teasley, H. E., Chang, H. J., Kim, T. H., Ku, B. J., and Jeong, J.-W. (2018) Expression of PIK3IP1 in the murine uterus during early pregnancy. *Biochem. Biophys. Res. Commun.* **495**, 2553–2558

20. Song, H. K., Kim, J., Lee, J. S., Nho, K. J., Jeong, H. C., Kim, J., Ahn, Y., Park, W. J., and Kim, D. H. (2015) Pik3ip1 modulates cardiac hypertrophy by inhibiting PI3K pathway. *PLoS ONE*. **10**, e0122251

21. Heng, T. S. P., Painter, M. W., and Immunological Genome Project Consortium (2008) The Immunological Genome Project: networks of gene expression in immune cells. *Nat. Immunol.* **9**, 1091–1094

22. Sidhom, J.-W., Theodros, D., Murter, B., Zarif, J. C., Ganguly, S., Pardoll, D. M., and Baras, A. (2019) ExCYT: A Graphical User Interface for Streamlining Analysis of High-Dimensional Cytometry Data. *J. Vis. Exp.* 10.3791/57473

23. Boulter, J. M., Schmitz, N., Sewell, A. K., Godkin, A. J., Bachmann, M. F., and Gallimore, A. M. (2007) Potent T cell agonism mediated by a very rapid TCR/pMHC interaction. *Eur. J. Immunol.* **37**, 798–806

24. Newton, A. C. (2018) Protein kinase C: perfectly balanced. *Crit. Rev. Biochem. Mol. Biol.* **53**, 208–230

25. Black, R. A., and White, J. M. (1998) ADAMs: focus on the protease domain. *Curr. Opin. Cell Biol.* **10**, 654–659

26. Pfeifhofer-Obermair, C., Thuille, N., and Baier, G. (2012) Involvement of distinct PKC gene products in T cell functions. *Front. Immunol.* **3**, 220

27. Müllberg, J., Schooltink, H., Stoyan, T., Heinrich, P. C., and Rose-John, S. (1992) Protein kinase C activity is rate limiting for shedding of the interleukin-6 receptor. *Biochem. Biophys. Res. Commun.* **189**, 794–800

28. Senior, A. W., Evans, R., Jumper, J., Kirkpatrick, J., Sifre, L., Green, T., Qin, C., Žídek, A., Nelson, A. W. R., Bridgland, A., Penedones, H., Petersen, S., Simonyan, K., Crossan, S., Kohli, P., Jones, D. T., Silver, D., Kavukcuoglu, K., and Hassabis, D. (2020) Improved protein structure prediction using potentials from deep learning. *Nature*. **577**, 706–710

29. Heo, L., and Feig, M. (2020) High-accuracy protein structures by combining machine-learning with physics-based refinement. *Proteins*. **88**, 637–642

30. Song, J., Wang, Y., Li, F., Akutsu, T., Rawlings, N. D., Webb, G. I., and Chou, K.-C. (2019) iProt-Sub: a comprehensive package for accurately mapping and predicting protease-specific substrates and cleavage sites. *Brief. Bioinformatics*. **20**, 638–658

31. Scheller, J., Chalaris, A., Garbers, C., and Rose-John, S. (2011) ADAM17: a molecular switch to control inflammation and tissue regeneration. *Trends Immunol.* **32**, 380–387

32. Zunke, F., and Rose-John, S. (2017) The shedding protease ADAM17: Physiology and pathophysiology. *Biochim. Biophys. Acta Mol. Cell Res.* **1864**, 2059–2070

33. Mishra, H. K., Ma, J., and Walcheck, B. (2017) Ectodomain Shedding by ADAM17: Its Role in Neutrophil Recruitment and the Impairment of This Process during Sepsis. *Front. Cell. Infect. Microbiol.* **7**, 138

34. Padmanabhan, K., Wu, T. P., Ravichandran, K. G., and Tulinsky, A. (1994) Kringle-kringle interactions in multimer kringle structures. *Protein Sci.* **3**, 898–910

35. Castellino, F. J., and McCance, S. G. (1997) The kringle domains of human plasminogen. *Ciba Found. Symp.* **212**, 46–60; discussion 60

36. Cibrián, D., and Sánchez-Madrid, F. (2017) CD69: from activation marker to metabolic gatekeeper. *Eur. J. Immunol.* **47**, 946–953

37. Rosse, C., Linch, M., Kermorgant, S., Cameron, A. J. M., Boeckeler, K., and Parker, P. J. (2010) PKC and the control of localized signal dynamics. *Nat. Rev. Mol. Cell Biol.* **11**, 103–112